KSME

Springer

Journal of Mechanical Science and Technology 38 (5) 2024

Original Article
DOI 10.1007/s12206-024-0406-4

Keywords:
· Active mount
· Active vibration control
· Automotive engine mount
· Noise vibration harshness
· Passive mount
· Piezoelectric stack actuator

Correspondence to:
Byeongil Kim
bikim@yu.ac.kr

Citation:
Hong, D., Moon, H., Kim, B. (2024). Bidirectional active vibration control of two-dimensional structure inspired by automotive engine mounting system. Journal of Mechanical Science and Technology 38 (5) (2024) 2231~2246. http://doi.org/10.1007/s12206-024-0406-4

Received September 24th, 2023
Revised January 9th, 2024
Accepted January 29th, 2024

† Recommended by Editor
No-cheol Park

Bidirectional active vibration control of two-dimensional structure inspired by automotive engine mounting system

Dongwoo Hong[1], Hojoon Moon[2] and Byeongil Kim[2]

[1]Daegu Mechatronics & Materials Institute, Daegu-si 42714, Korea, [2]School of Mechanical Engineering, Yeungnam University, Gyeongsan-si, Gyeongsangbuk-do 38541, Korea

Abstract Recently, active mounting systems have been applied to automotive engine mounts to effectively mitigate structure-borne vibrations throughout the vehicle chassis. Active mounting systems have been investigated extensively to alleviate the vibration and noise of automobiles; however, the actual engine mounting orientation is not considered, and only an extremely small range of specific vibration and noise control is examined. This paper presents the modeling, analysis, and control of a source structure with an active mounting system while considering the location and direction of actual automotive engine mounts. Two active mounts comprising a piezoelectric stack actuator arranged in series with an elastomeric mount are applied to mitigate both vertical and horizontal vibrations by setting a variable parameter via the dynamic relation of the source structure. When harmonic excitation forces are employed, the secondary force required by each active mount can be calculated mathematically, and a control signal is applied to reduce vibrations through destructive interference with the input signal. Simulation results show that the excitation vibration can be reduced using this bidirectional active mount. Hence, noise vibration harshness is expected to be improved by controlling the vibration of the actual automotive engine structure and the secondary force of actuators.

1. Introduction

Vibration and noise are generated during the operation of most mechanical devices, thus degrading machine performance in terms of reliability and durability. Owing to the current rapid growth of technology, not only the performance satisfaction toward a product, but also the emotional pleasure derived through the five senses of humans must be fulfilled. Based on automobiles, a representative emotional product, as an example, the durability, fuel economy, and crash performance of vehicles are regarded as crucial throughout the previous automobile development stage, whereas consumers have recently demanded ride comfort and improvement in noise vibration harshness (NVH). The development of electric vehicles (EVs) necessitates the control of the noise and vibration of vehicles, which is difficult owing to the excitation force that emerges in the motor, gearbox, and inverter, as compared with the excitation force in the internal combustion engine. Therefore, the appropriate research and design must be conducted toward engine mounts that can sustain the powertrain of a vehicle and isolate a vehicle from vibrations conveyed by the powertrain. Passive engine mounting techniques are currently utilized in most commercial vehicles to adequately isolate lateral, vertical, and longitudinal vibrations in the low-frequency range, as shown in Fig. 1(a). However, they cannot isolate vibrations at high frequencies from EVs, as shown in Fig. 1(b). Consequently, smart structure-based active engine mounting technology, which can improve ride comfort and NVH in a variable environment by modifying mount dynamics to accommodate low- or high-frequency ranges, has garnered significant interest as a key technology in the field of automobile development.

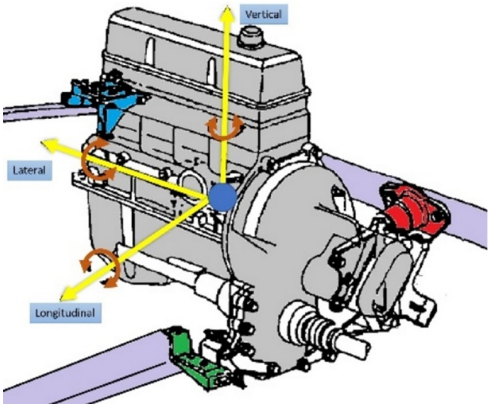

(a)

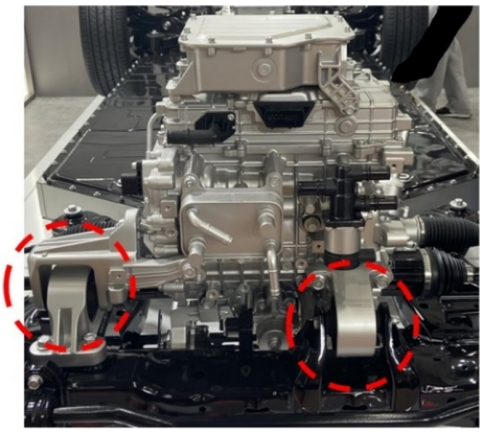

(b)

Fig. 1. (a) Automotive engine vibration; (b) EV mounts.

1.1 Literature review

An engine mount supports the powertrain of a vehicle and prevents the vibrations generated by the powertrain from being transmitted to the vehicle body. Conventionally, rubber, which is viscoelastic, is used; however, it can provide insulation only in the low-frequency region and cannot control vibrations in the high-frequency region. Recently, the automobile industry has investigated significantly in the commercialization of EVs; thus, studies are being conducted actively to control the more complex external forces generated from motors and gearboxes as compared to those from existing internal combustion engines. Yu et al. [1] briefly explained the principles and limitations of passive, semi-active, and active mounts. Representative passive mounts include elastic mounts and manual hydraulic mounts, which control vibrations effectively in the low-frequency range, but not in the high-frequency range. Semi-active mounts typically feature mounts using electrorheological (ER) and magnetorheological (MR) fluids, which demonstrate better vibration control performance than passive mounts in the low-frequency range but cannot control vibrations in the high-frequency range. Representative active mounts include elastic and hydraulic mounts that combine an actuator with an existing passive mount. Vibrations in the high- and low-frequency bands can be controlled by adjusting the dynamic stiffness via the actuator for each band. Hosseini et al. [2] developed a nonlinear model of a motor mount with a solenoid actuator and an experimental model. Kraus et al. [3] demonstrated that an engine mount can be fabricated by connecting a viscous damper and an actuator in series; their model reduced noise and vibration. Chae et al. [4] applied an MR damper to the ambulance bed stage to reduce vibrations. Yang et al. [5] utilized an adaptive multinotch filtered algorithm to perform vibration isolation on four hydraulic actuators. Jeon et al. [6] proposed a new controllable engine mounting system using a magnetorheological fluid actuator for the roll mount and a piezo stack actuator for the RH mount. Jiang et al. [7] conducted experiments utilizing a magnetostrictive actuator for active vibration control. Using experiments and simulations, Fakhari et al. [8] applied a robust model reference adaptive control to an electromagnetic engine mount and demonstrated isolation. Elahinia et al. [9] presented a semi-active actuator with magnetorheological and electrorheological fluids, demonstrating efficacy in shock and vibration isolation. Wu et al. [10] devised a vibration insulator using the high-static-low-dynamic stiffness (MS-NS) characteristics of a magnetic spring with negative stiffness. A hydraulic engine mount was mathematically modeled and simulated by Truong [11]. Kamada et al. [12] demonstrated that a structure's vibration can be effectively isolated by integrating a column and piezoelectric actuator for active vibration control. Loukil et al. [13] proposed a method for utilizing the power of a piezo actuator via energy harvesting, demonstrating effective isolation performance. Sui et al. [14] fabricated a vehicle engine mount using PZT with rapid response characteristics, and they demonstrated vibration reduction performance via simulation.

Choi and Choi [15] developed a sliding-mode controller (SMC) and compared its vibration reduction performance with that of a shear mode-type ER fluid engine mount. They showed that the vibration response reduced when an SMC with a varying electric field was used as the input current, as compared with using a constant electric field. Sarkar et al. [16] presented a theory for designing an ideal engine mount using an MR fluid, where vibrations in all frequency ranges were reduced by controlling the dynamic stiffness of the MR fluid via magnetic field control to obstruct the flow of the MR fluid. However, controlling the fluid was challenging and fluid leakage occurred when the fluid was used in an engine mount. Chang et al. [17] incorporated the quasi-zero-stiffness method into the existing dynamic vibration absorber (DVA) method to control the anti-resonance generated at ultralow frequencies (2.3 Hz), which cannot not be controlled by DVAs alone. Liette et al. [18] demonstrated vehicle vibration and noise reduction in the frequency band of the power electric of a hybrid vehicle using an active mount that combines a piezoelectric (PZT) stack actuator and a rubber mount in series. In addition, Hong and Kim [19, 20] conducted an analytical study on a mounting system using one active mount and two rubber mounts as well as combining

a PZT stack actuator and a rubber mount on a vehicle model with a plate structure; their results confirmed the applicability of the system. Hong and Kim [21] also developed a quantification method for determining ideal inputs for active structural paths analytically. Derived inputs work well numerically, while they should be tuned a little experimentally.

Qiu et al. [22] confirmed vibration reduction based on the change in the position of a PZT stack actuator in a plate structure model and proposed criteria for the location of the active mount to reduce vibration. This may be an optimal method for solving fluid leakage and uncontrollability in the high-frequency region of the existing mounting system. Furthermore, it exploits the low power and rapid response of the PZT actuator. To utilize active engine mounts (AEMs), the controller must be considered. Hausberg et al. [23] theoretically and experimentally analyzed the secondary path change in an AEM and predicted the dynamic characteristics of an AEM using the Fx-LMS (filtered-x least mean squares) algorithm, which is an adaptive filter. Kraus et al. [24] fabricated a vehicle engine mount by combining an actuator and a viscoelastic mount and investigated it experimentally. The actuator input value used in the experiment was controlled by applying the response generated from the mass of the vehicle engine mount using the Fx-LMS algorithm. The experimental results showed that vibration and noise reduced. Bartel et al. [25] proposed an innovative type of engine mount designed to withstand dynamic forces. The results demonstrated that the proposed engine mount could be used to isolate vibrations. There are several research efforts for realizing active control based on skyhook damping. Li and Goodall [26] investigated several control methodologies for employing skyhook damping control applied for railway vehicles' active suspension systems. The absolute velocity signal is filtered using nonlinear techniques based upon Kalman-filters. Singal and Rajamani [27] proposed a novel zero-energy active suspension system with an energy adaptive skyhook gain. This approach showed that the system acts not only as a passive system for all frequencies, but also as an active system for a broad range of frequencies. Emura et al. [28] developed a semi-active suspension system with skyhook damping for actively controlling the damping coefficient and its system configuration. Chai et al. investigated the active control application on composite lattice sandwich plates with piezoelectric actuator and sensor. The nonlinear equations are utilized to obtain plates' response and the velocity feedback and H-infinity controllers are applied [29]. Kim et al. developed two different enhanced LMS algorithm based on the sliding mode controller and applied them to a simple smart structure to validate the vibration control performance [30, 31]. Since newly developed control schemes can adequately manage relatively complex signals such as incommensurate and modulated signals, it can be implemented to active control applications for next generation mobilities.

1.2 Research purpose

Various types of smart materials have been proposed for the vibration insulation of vehicle engines. Among the smart structure-based engine mounting systems used for vibration isolation, the semi-active mounting system using ER and MR fluids cannot effectively control vibrations over a wide frequency band owing to the nature of the fluids, and fluid leakage is imminent. Hence, an active mounting system combining a PZT actuator and rubber, which is a viscoelastic material, was proposed. Furthermore, a method for reducing vibrations using an adaptive filter as an input signal to the actuator and for monitoring the response signal of the system was proposed. In addition, a method of changing the structure when a single frequency is excited or reducing narrow-band vibrations was proposed; however, this method is not suitable for EVs with complex signals generated from the gearbox, transmission, and motor. Not like the schematic presented in Fig. 2, the passive elastomeric bearings can be put in parallel to the piezoelectric actuators. If then, it will make one path to two paths, because those two will be apart physically at any way. This makes the modeling and the quantification of actuator input more complicated. Simpler model with enough assumptions will make the results clear and it can be a basis to more detailed investigation thereafter. Also, a laboratory-based test would be carried out and the results will be discussed in the authors' next research paper. In that sense, if the piezoelectric actuator is put in parallel, it would make the experimental setup too large.

Previous literatures have focused on the active mounting systems itself and investigated the vibration attenuation performance in one direction only. Actual engine mounting orientation consists of longitudinal, lateral, and vertical directions, as

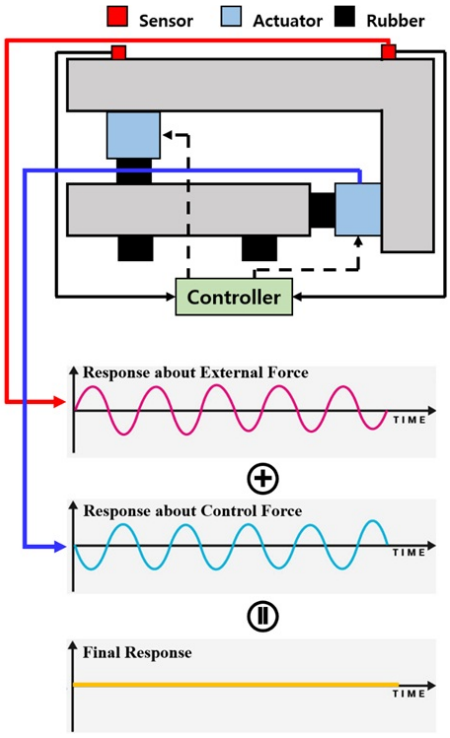

Fig. 2. Active vibration control system applied to automotive mounts.

described in Fig. 1(a) and the structure of the active mounting system in this article have two mounts (vertical and lateral), as shown in Fig. 2.

Therefore, in this study, the source–path–receiver structure is designed while considering the combination of vehicle engine mounts in the vertical and horizontal directions. Subsequently, the amount of vibration reduced is observed using a PZT stack actuator and an active mount coupled with rubber, as shown in Fig. 2.

The remainder of this paper is organized as follows: In Sec. 2, a two-dimensional 7-degree-of-freedom (DOF) model is proposed, which features active mounts combined in the vertical and horizontal directions to reduce vibration. In Sec. 3, when the structure is excited with a single sinusoid, the input value for each path is calculated analytically, and the abatement is compared. Finally, the results of this study and future research directions are summarized in Sec. 5.

2. Vertical and horizontal active mounting systems for vibration reduction

2.1 Lumped parameter modeling

The vehicle engine, AEM, and subframe structure are shown in Fig. 3. The engine is defined as the source, the piezostack actuator and rubber-coupled active mount as the paths, and the subframe as the receiver. As the engine mount in an actual vehicle is horizontally coupled to the engine and subframe, the source was designed as a curved two-dimensional structure, and the receiver was designed as a simple two-dimensional structure.

In the figure, m_1 represents the mass of the source, m_2 the mass of the receiver, m_{ac1} the mass of the actuator in the vertical direction, and m_{ac2} the mass of the actuator in the horizontal direction. I_1^y and I_2^y represent the moments of inertia in the y-direction of the source and receiver, respectively. l_{si} and l_{ri} represent the distance between each path from the centers of gravity of the source and receiver, respectively; and d represents the distance from the center of gravity of the source to the location where the excitation force is applied. k_{mi}^{*z} and k_{mi}^{*x} are the vertical (z-direction) and horizontal (x-direction) complex stiffnesses between the source or receiver and the paths, respectively; and k_{bi}^{*z} is the stiffness between the receiver and floor, which represents the complex stiffness. In this study, a 7-DOF model was assumed, considering the vertical translation of the source and receiver, y-axis rotation, vertical translation of vertically connected active mounts, and vertical and horizontal translations of horizontally connected active mounts. Therefore, the displacement vector represents the vertical displacement of the source (ε_1^z), rotation angle (θ_1^y), vertical displacement (ε_2^z), rotation angle (θ_2^y), vertical displacement of the vertically active mount (ε_{ac1}^z), and the vertical displacement (ε_{ac2}^z) and horizontal displacement (ε_{ac2}^x) of the horizontally active mount. ε_{ac1}^z is the excitation force, f_{ac1}^z the control force of the vertically active mount, and f_{ac2}^x the control force of the horizontally active mount. The equation of motion for the model above can be derived using Newton's second law, as shown in Eq. (1).

$$M\ddot{q} + C\dot{q} + K^* q = W + F \tag{1}$$

where q is the displacement vector, M the mass matrix, K^* the complex stiffness matrix, C the damping matrix, W the excitation force vector, and F the control force vector of the active mount. Because an active mount combined with rubber, which is a damping material, is used in addition to a piezostack, the complex stiffness can be expressed in terms of damping and stiffness using the Kelvin–Voigt model, which is expressed as shown in Eq. (2).

$$k^* = k\left(1 + (\omega c / k)\, j\right). \tag{2}$$

The real-valued stiffness and damping are calculated using the equation above. When expressed based on the Kelvin–Voigt model shown in Fig. 4, seven equations of motion are as follows, expressed in Eqs. (3)-(9).

$$\begin{aligned} &m_1\ddot{\varepsilon}_1^z + \left(c_{m1}^z + c_{m2}^z\right)\dot{\varepsilon}_1^z - c_{m1}^z\dot{\varepsilon}_{ac1}^z - c_{m2}^z\dot{\varepsilon}_{ac2}^z + c_{m2}^{zx}\dot{\varepsilon}_{ac2}^x \\ &+\left(c_{m2}^z l_{s2} - c_{m1}^z l_{s1} - c_{m2}^{zx} l_{s3}\right)\dot{\theta}_1^y + \left(k_{m1}^{*z} + k_{m2}^{*z}\right)\varepsilon_1^z \\ &-k_{m1}^{*z}\varepsilon_{ac1}^z - k_{m2}^{*z}\varepsilon_{ac2}^z + k_{m2}^{*zx}\varepsilon_{ac2}^x + (k_{m2}^{*z} l_{s2} - k_{m1}^{*z} l_{s1} \\ &-k_{m2}^{*zx} l_{s3})\theta_1^y = W^z \end{aligned} \tag{3}$$

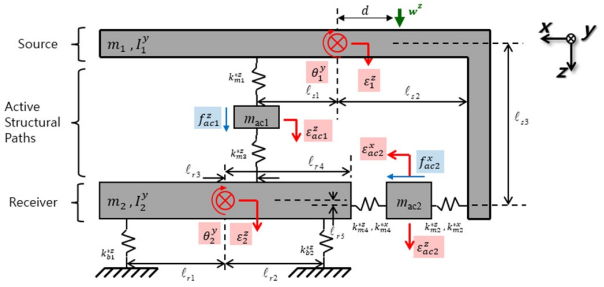

Fig. 3. Model of source–path–receiver with complex stiffness.

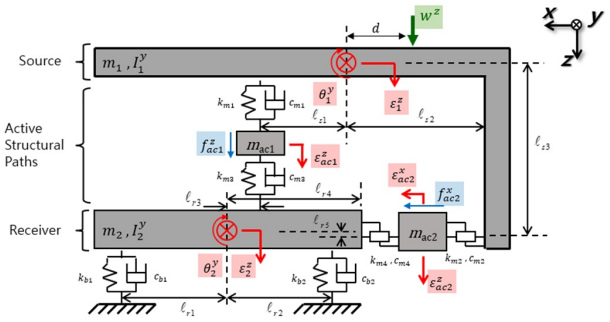

Fig. 4. Mathematical modeling of 7-DOF system based on Kelvin–Voigt model.

$$
\begin{aligned}
&m_2\ddot{\varepsilon}_2^z+\left(c_{m3}^z+c_{m4}^z+c_{b1}^z+c_{b2}^z\right)\dot{\varepsilon}_2^z-c_{m3}^z\dot{\varepsilon}_{ac1}^z-c_{m4}^z\dot{\varepsilon}_{ac2}^z\\
&+c_{m4}^{zx}\dot{\varepsilon}_{ac2}^x+\left(c_{m3}^z l_{r3}+c_{m4}^z l_{r4}-c_{b1}^z l_{r1}+c_{b2}^z l_{r2}-c_{m4}^{zx} l_{r5}\right)\\
&\dot{\theta}_2^y+\left(k_{m3}^{*z}+k_{m4}^{*z}+k_{b1}^{*z}+k_{b2}^{*z}\right)\varepsilon_2^z-k_{m3}^{*z}\varepsilon_{ac1}^z-k_{m4}^{*z}\varepsilon_{ac2}^z\\
&+k_{m4}^{*zx}\varepsilon_{ac2}^x+\left(k_{m3}^{*z} l_{r3}+k_{m4}^{*z} l_{r4}-k_{b1}^{*z} l_{r1}+k_{b2}^{*z} l_{r2}-k_{m4}^{*zx} l_{r5}\right)\theta_2^y=0
\end{aligned}
\tag{4}
$$

$$
\begin{aligned}
&m_{ac1}\ddot{\varepsilon}_{ac1}^z-c_{m1}^z\dot{\varepsilon}_1^z-c_{m3}^z\dot{\varepsilon}_2^z+\left(c_{m1}^z+c_{m3}^z\right)\dot{\varepsilon}_{ac1}^z+c_{m1}^z l_{s1}\dot{\theta}_1^y\\
&-c_{m3}^z l_{r3}\dot{\theta}_2^y-k_{m1}^{*z}\varepsilon_1^z-k_{m3}^{*z}\varepsilon_2^z+\left(k_{m1}^{*z}+k_{m3}^{*z}\right)\varepsilon_{ac1}^z\\
&+k_{m1}^{*z} l_{s1}\theta_1^y-k_{m3}^{*z} l_{r3}\theta_2^y=f_{ac1}^z
\end{aligned}
\tag{5}
$$

$$
\begin{aligned}
&m_{ac2}\ddot{\varepsilon}_{ac2}^z-c_{m2}^z\dot{\varepsilon}_1^z-c_{m4}^z\dot{\varepsilon}_2^z+\left(c_{m2}^z+c_{m4}^z\right)\dot{\varepsilon}_{ac2}^z\\
&-\left(c_{m2}^{zx}+c_{m4}^{zx}\right)\dot{\varepsilon}_{ac2}^x+\left(c_{m2}^{zx} l_{s3}-c_{m2}^z l_{s2}\right)\dot{\theta}_1^y\\
&+\left(c_{m4}^{zx} l_{r5}-c_{m4}^z l_{r4}\right)\dot{\theta}_2^y-k_{m2}^{*z}\varepsilon_1^z-k_{m4}^{*z}\varepsilon_2^z+(k_{m2}^{*z}\\
&+k_{m4}^{*z})\varepsilon_{ac2}^z-\left(k_{m2}^{*zx}+k_{m4}^{*zx}\right)\varepsilon_{ac2}^x+\left(k_{m2}^{*zx} l_{s3}-k_{m2}^{*z} l_{s2}\right)\theta_1^y\\
&+\left(k_{m4}^{*zx} l_{r5}-k_{m4}^{*z} l_{r4}\right)\theta_2^y=0
\end{aligned}
\tag{6}
$$

$$
\begin{aligned}
&m_{ac2}\ddot{\varepsilon}_{ac2}^x+c_{m2}^{zx}\dot{\varepsilon}_1^z+c_{m4}^{zx}\dot{\varepsilon}_2^z-\left(c_{m2}^{zx}+c_{m4}^{zx}\right)\dot{\varepsilon}_{ac2}^z\\
&+\left(c_{m2}^x+c_{m4}^x\right)\dot{\varepsilon}_{ac2}^x+\left(c_{m2}^{zx} l_{s2}-c_{m2}^x l_{s3}\right)\dot{\theta}_1^y\\
&+\left(c_{m4}^{zx} l_{r4}-c_{m4}^x l_{r5}\right)\dot{\theta}_2^y+k_{m2}^{*zx}\varepsilon_1^z+k_{m4}^{*zx}\varepsilon_2^z-(k_{m2}^{*zx}\\
&+k_{m4}^{*zx})\varepsilon_{ac2}^z+\left(k_{m2}^{*x}+k_{m4}^{*x}\right)\varepsilon_{ac2}^x+\left(k_{m2}^{*zx} l_{s2}-k_{m2}^{*x} l_{s3}\right)\theta_1^y\\
&+\left(k_{m4}^{*zx} l_{r4}-k_{m4}^{*x} l_{r5}\right)\theta_2^y=f_{ac2}^x
\end{aligned}
\tag{7}
$$

$$
\begin{aligned}
&I_1^y\ddot{\theta}_1^y+\left(c_{m2}^z l_{s2}-c_{m2}^{zx} l_{s3}-c_{m1}^z l_{s1}\right)\dot{\varepsilon}_1^z+c_{m1}^z l_{s1}\dot{\varepsilon}_{ac1}^z\\
&+\left(c_{m2}^{zx} l_{s3}-c_{m2}^z l_{s2}\right)\dot{\varepsilon}_{ac2}^z+\left(c_{m2}^{zx} l_{s2}-c_{m2}^x l_{s3}\right)\dot{\varepsilon}_{ac2}^x+(c_{m1}^z l_{s1}^2\\
&+c_{m2}^z l_{s2}^2+c_{m2}^x l_{s3}^2-2c_{m2}^{zx} l_{s2} l_{s3})\dot{\theta}_1^y+(k_{m2}^{*z} l_{s2}-k_{m2}^{*zx} l_{s3}\\
&-k_{m1}^{*z} l_{s1})\varepsilon_1^z+k_{m1}^{*z} l_{s1}\varepsilon_{ac1}^z+\left(k_{m2}^{*zx} l_{s3}-k_{m2}^{*z} l_{s2}\right)\varepsilon_{ac2}^z\\
&+\left(k_{m2}^{*zx} l_{s2}-k_{m2}^{*x} l_{s3}\right)\varepsilon_{ac2}^x+\left(k_{m1}^{*z} l_{s1}^2+k_{m2}^{*z} l_{s2}^2+k_{m2}^{*x} l_{s3}^2-2k_{m2}^{*zx} l_{s2} l_{s3}\right)\\
&\theta_1^y=W^z d
\end{aligned}
\tag{8}
$$

$$
\begin{aligned}
&I_2^y\ddot{\theta}_2^y+\left(c_{m3}^z l_{r3}+c_{m4}^z l_{r4}-c_{b1}^z l_{r1}+c_{b2}^z l_{r2}-c_{m4}^{zx} l_{r5}\right)\dot{\varepsilon}_2^z\\
&-c_{m3}^z l_{r3}\dot{\varepsilon}_{ac1}^z+\left(-c_{m4}^z l_{r4}+c_{m4}^{zx} l_{r5}\right)\dot{\varepsilon}_{ac2}^z\\
&+\left(-c_{m4}^x l_{r5}+c_{m4}^{zx} l_{r4}\right)\dot{\varepsilon}_{ac2}^x\\
&+\left(c_{m3}^z l_{r3}^2+c_{m4}^z l_{r4}^2+c_{m4}^x l_{r5}^2+c_{b1}^z l_{r1}^2+c_{b2}^z l_{r2}^2-2c_{m4}^{zx} l_{r5} l_{r4}\right)\\
&\dot{\theta}_2^y+(k_{m3}^{*z} l_{r3}+k_{m4}^{*z} l_{r4}-k_{b1}^{*z} l_{r1}+k_{b2}^{*z} l_{r2}-k_{m4}^{*zx} l_{r5})\\
&\varepsilon_2^z-k_{m3}^{*z} l_{r3}\varepsilon_{ac1}^z+\left(-k_{m4}^{*z} l_{r4}+k_{m4}^{*zx} l_{r5}\right)\varepsilon_{ac2}^z\\
&+\left(-k_{m4}^{*x} l_{r5}+k_{m4}^{*zx} l_{r4}\right)\varepsilon_{ac2}^x+(k_{m3}^{*z} l_{r3}^2+k_{m4}^{*z} l_{r4}^2+k_{m4}^{*x} l_{r5}^2\\
&+k_{b1}^{*z} l_{r1}^2+k_{b2}^{*z} l_{r2}^2-2k_{m4}^{*zx} l_{r5} l_{r4})\theta_2^y=0\,.
\end{aligned}
\tag{9}
$$

In addition, the mass matrix, complex stiffness matrix, damping matrix, displacement vector, excitation force vector, and control force vector are expressed as shown in Eqs. (10)-(15).

$$
M=diag\left(\begin{bmatrix} m_1 & m_2 & m_{ac1} & m_{ac2} & m_{ac2} & I_1^y & I_2^y \end{bmatrix}\right) \tag{10}
$$

$$
K^*=\begin{bmatrix}
k_{m1}^{*z}+k_{m2}^{*z} & 0 & -k_{m1}^{*z} & -k_{m2}^{*z} & k_{m2}^{*zx} & k_{m2}^{*zx} & k_{m1}^{*z} & -k_{m2}^{*z} & k_{m2}^{*zx} & k_{m2}^{*z} l_{s2}-k_{m1}^{*z} l_{s1}-k_{m2}^{*zx} l_{s3} & 0 & k_{m1}^{*z} l_{s1} & k_{m2}^{*zx} l_{s3}-k_{m2}^{*z} l_{s2} & k_{m2}^{*zx} l_{s2}-k_{m2}^{*x} l_{s3} & k_{m1}^{*z} l_{s1}^2+k_{m2}^{*z} l_{s2}^2+k_{m2}^{*x} l_{s3}^2-2k_{m2}^{*zx} l_{s2} l_{s3} & 0\\
0 & k_{m3}^{*z}+k_{m4}^{*z}+k_{b1}^{*z}+k_{b2}^{*z} & -k_{m3}^{*z} & -k_{m4}^{*z} & k_{m4}^{*zx} & 0 & -k_{m4}^{*z} & k_{m4}^{*zx} & 0 & k_{m3}^{*z} l_{r3}+k_{m4}^{*z} l_{r4}-k_{b1}^{*z} l_{r1}+k_{b2}^{*z} l_{r2}-k_{m4}^{*zx} l_{r5} & 0 & 0 & 0 & 0 & 0 & k_{m3}^{*z} l_{r3}^2+k_{m4}^{*z} l_{r4}^2+k_{m4}^{*x} l_{r5}^2+k_{b1}^{*z} l_{r1}^2+k_{b2}^{*z} l_{r2}^2-2k_{m4}^{*zx} l_{r5} l_{r4}
\end{bmatrix} \tag{11}
$$

$$
C=\begin{bmatrix}
c_{m1}^z+c_{m2}^z & 0 & -c_{m1}^z & -c_{m2}^z & c_{m2}^{zx} & c_{m2}^{zx} & c_{m1}^z & -c_{m2}^z & c_{m2}^{zx} & c_{m2}^z l_{s2}-c_{m2}^{zx} l_{s3}-c_{m1}^z l_{s1} & 0 & c_{m1}^z l_{s1} & c_{m2}^{zx} l_{s3}-c_{m2}^z l_{s2} & c_{m2}^{zx} l_{s2}-c_{m2}^x l_{s3} & c_{m1}^z l_{s1}^2+c_{m2}^z l_{s2}^2+c_{m2}^x l_{s3}^2-2c_{m2}^{zx} l_{s2} l_{s3} & 0\\
0 & c_{m3}^z+c_{m4}^z+c_{b1}^z+c_{b2}^z & -c_{m3}^z & -c_{m4}^z & c_{m4}^{zx} & 0 & -c_{m4}^z & c_{m4}^{zx} & 0 & c_{m3}^z l_{r3}+c_{m4}^z l_{r4}-c_{b1}^z l_{r1}+c_{b2}^z l_{r2}-c_{m4}^{zx} l_{r5} & 0 & 0 & 0 & 0 & 0 & c_{m3}^z l_{r3}^2+c_{m4}^z l_{r4}^2+c_{m4}^x l_{r5}^2+c_{b1}^z l_{r1}^2+c_{b2}^z l_{r2}^2-2c_{m4}^{zx} l_{r5} l_{r4}
\end{bmatrix}
$$

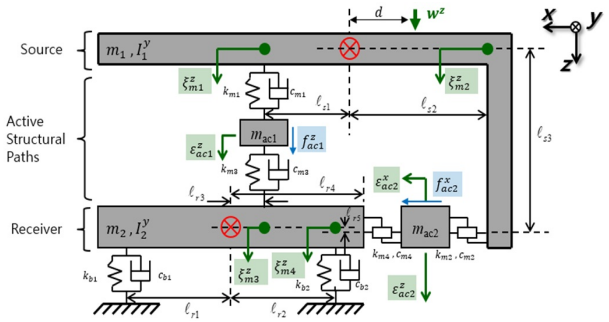

Fig. 5. 7-DOF modeling based on mount coordinates.

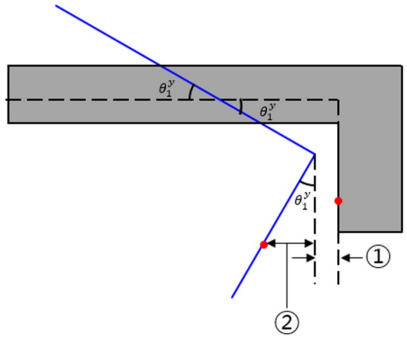

Fig. 6. Dynamic movement of source by external force.

$$\begin{bmatrix} 0 \\ c_{m3}^{z}l_{r3}+c_{m4}^{z}l_{r4}-c_{b1}^{z}l_{r1}+c_{b2}^{z}l_{r2}-c_{m4}^{zx}l_{r5} \\ -c_{m3}^{z}l_{r3} \\ c_{m4}^{zx}l_{r5}-c_{m4}^{z}l_{r4} \\ c_{m4}^{zx}l_{r4}-c_{m4}^{x}l_{r5} \\ 0 \\ c_{m3}^{z}l_{r3}^{2}+c_{m4}^{z}l_{r4}^{2}+c_{m4}^{x}l_{r5}^{2}+c_{b1}^{z}l_{r1}^{2}+c_{b2}^{z}l_{r2}^{2}-2c_{m4}^{zx}l_{r5}l_{r4} \end{bmatrix} \tag{12}$$

$$q=\begin{bmatrix} \varepsilon_1^z & \varepsilon_2^z & \varepsilon_{ac1}^z & \varepsilon_{ac2}^z & \varepsilon_{ac2}^x & \theta_1^y & \theta_2^y \end{bmatrix}^T \tag{13}$$

$$W=\begin{bmatrix} W^z & 0 & 0 & 0 & 0 & W^z d & 0 \end{bmatrix}^T \tag{14}$$

$$F=\begin{bmatrix} 0 & 0 & f_{ac1}^z & 0 & f_{ac2}^x & 0 & 0 \end{bmatrix}^T. \tag{15}$$

The model designed using the coordinates of the center of gravity was converted into mount coordinates to analyze the displacement of the position adjacent to the mount.

In Fig. 5, ξ_{m1}^z is the vertical displacement of the source adjacent to the vertical mount; ξ_{m2}^z is the vertical displacement of the source adjacent to the horizontal mount; ξ_{m3}^z is the vertical displacement of the receiver adjacent to the vertical mount; and ξ_{m4}^z is the vertical displacement of the receiver adjacent to the vertical mount, which indicates the vertical displacement of the adjacent receiver. A transformation matrix for converting the center of gravity (CG) coordinates into the mount coordinates can be expressed using the internal division formula shown in Eq. (16).

$$\varepsilon_1^z=\frac{\xi_{m1}^z l_{s2}+\xi_{m2}^z l_{s1}}{l_{s1}+l_{s2}}=\frac{l_{s2}}{l_{s1}+l_{s2}}\xi_{m1}^z+\frac{l_{s1}}{l_{s1}+l_{s2}}\xi_{m2}^z. \tag{16}$$

$$\Pi=\begin{bmatrix} \frac{l_{s2}}{l_{s1}+l_{s2}} & \frac{l_{s1}}{l_{s1}+l_{s2}} & 0 & 0 & 0 & 0 & 0 \\ 0 & 0 & 0 & 0 & 0 & \frac{l_{r4}}{l_{r3}+l_{r4}} & \frac{l_{r3}}{l_{r3}+l_{r4}} \\ 0 & 0 & 1 & 0 & 0 & 0 & 0 \\ 0 & 0 & 0 & 1 & 0 & 0 & 0 \\ 0 & 0 & 0 & 0 & 1 & 0 & 0 \\ -\frac{1}{l_{s1}+l_{s2}} & \frac{1}{l_{s1}+l_{s2}} & 0 & 0 & 0 & 0 & 0 \\ 0 & 0 & 0 & 0 & 0 & -\frac{1}{l_{r3}+l_{r4}} & \frac{1}{l_{r3}+l_{r4}} \end{bmatrix} \tag{17}$$

Using this transformation matrix, the displacement vector of the mount coordinates can be obtained, as shown in Eq. (18). The equation of motion transformed into the mount coordinates is obtained by multiplying the transformation matrix by the mass, damping, and stiffness matrices of the CG coordinates, as shown in Eq. (19).

$$q'=\begin{bmatrix} \xi_{m1}^z & \xi_{m2}^z & \varepsilon_{ac1}^z & \varepsilon_{ac2}^z & \varepsilon_{ac2}^x & \xi_{m3}^z & \xi_{m4}^z \end{bmatrix}^T \tag{18}$$

$$\ddot{M}'\ddot{q}'+C'\dot{q}'+K'q'=W+F. \tag{19}$$

By converting this equation of motion to the mount coordinates, the vibration reduction performance of the active mount can be effectively investigated.

2.2 Horizontal displacement trend based on dynamic relations

Using the proposed lumped-parameter model, the response in the horizontal direction cannot be determined, whereas the response in the vertical direction at each position can be obtained. Therefore, in this study, the horizontal direction response trend of each position was calculated using the dynamic relationship of the structure, and the horizontal direction response trend of the position adjacent to the horizontal mount, which significantly affected the horizontal direction displacement, was identified. The dynamic movement of the source structure is illustrated in Fig. 6.

The dotted line in the figure above represents the equilibrium state of the source, and the solid line represents the movement of the source owing to external forces. The displacement of the source adjacent to the horizontal mount can be expressed as the sum of ① and ②, where ① can be derived from the characteristics of an isosceles triangle and the trigonometric formula shown in Eq. (20), whereas ② can be determined from the ratio of the similitude, as expressed in Eq. (21).

$$11=\xi_{m2}^z tan\left(\frac{\theta_1^y}{2}\right) \tag{20}$$

$$22:\xi_{m2}^z=l_{s3}sin\left(\theta_1^y\right):l_{s2}sin\left(\theta_1^y\right). \tag{21}$$

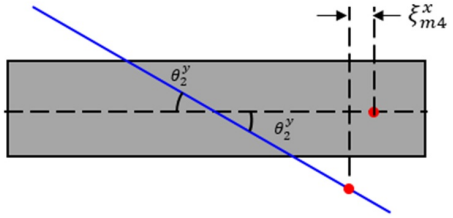

Fig. 7. Dynamic movement of receiver by external force.

Based on Eqs. (20) and (21), the displacement trend in the horizontal direction of the source adjacent to the horizontal mount can be expressed as shown in Eq. (22).

$$\xi^x_{m2} = \left(tan\left(\frac{\theta^y_1}{2}\right) + \frac{l_{s2}}{l_{s3}} \right) \xi^z_{m2} . \tag{22}$$

By linearizing Eqs. (22) and (23) can be obtained.

$$\xi^x_{m2} = \left(\frac{\theta^y_1}{2} + \frac{l_{s2}}{l_{s3}} \right) \xi^z_{m2} . \tag{23}$$

Based on the equations above, the horizontal displacement of the source is affected by the structure shape, rotation angle of the source, and vertical displacement. Because the source structure cannot be changed easily, the horizontal displacement of the source should be controlled through vertical displacement. The dynamic movements of the receiver structure are illustrated in Fig. 7.

The dotted line in Fig. 7 represents the equilibrium state of the receiver, and the solid line represents the movement of the receiver owing to external forces. The displacement of the receiver adjacent to the horizontal mount is denoted as ξ^x_{m4}, which is equivalent to ① for deriving the horizontal displacement of the source using the characteristics of an isosceles triangle and the formula of a trigonometric function, i.e.,

$$\xi^x_{m4} = \xi^z_{m4} tan\left(\frac{\theta^y_2}{2}\right). \tag{24}$$

By linearizing Eqs. (24) and (25) can be obtained.

$$\xi^x_{m4} = \frac{\theta^y_2}{2} \xi^z_{m4} . \tag{25}$$

This equation shows that the receiver's horizontal displacement is affected by its rotation angle and vertical displacement. Therefore, it can be controlled using the horizontal displacement of the receiver. Thus, the responses in the vertical and horizontal directions of the 7-DOF model were investigated.

3. Quantification of secondary pathway input

When the structure is excited by a harmonic force, both the amplitude and phase values affect the response. In addition, the excitation and control forces can be expressed in the form of a complex number using Euler's law, as expressed in Eqs. (26)-(28).

$$W^{z*}(t) = W^z e^{i\omega t} \tag{26}$$

$$f^{z*}_{ac1}(t) = f^z_{ac1} e^{i(\omega t + \phi_{ac1})} \tag{27}$$

$$f^{x*}_{ac2}(t) = f^x_{ac2} e^{i(\omega t + \phi_{ac2})} . \tag{28}$$

In the equation above, W^z is the amplitude of excitation force, ω the excitation frequency, f^z_{ac1} the amplitude the vertical control force, ϕ_{ac1} the phase of the vertical control force, f^x_{ac2} the amplitude of the horizontal control force, and ϕ_{ac2} the phase of the horizontal control force. The response at each position can be obtained by applying the excitation and control forces to the mount coordinate model. The response of each position is represented by the Eq. (29).

$$\xi^*_i(t) = \xi^{z*}_{mi}(t) . \tag{29}$$

Here, $\xi^{z*}_{mi}(t)$ is the vertical displacement of the ith-position of the mount coordinates, which is a response affected by the excitation force and the control force input through the secondary path. This can be determined by using the compliance matrix, which is defined as the inverse of the dynamic stiffness matrix. Based on the mount coordinates, the dynamic stiffness matrix can be obtained using Eq. (30), and the compliance matrix can be expressed as shown in Eq. (31).

$$\left[\kappa^{*'}\right] = -\omega^{2'} M' + i\omega C' + K' \tag{30}$$

$$\mathrm{H}^{*'} = \left[\kappa^{*'}\right]^{-1} = \begin{bmatrix} H^{*'}_{11} & H^{*'}_{12} & H^{*'}_{13} & H^{*'}_{14} & H^{*'}_{15} & H^{*'}_{16} & H^{*'}_{17} \\ H^{*'}_{21} & H^{*'}_{22} & H^{*'}_{23} & H^{*'}_{24} & H^{*'}_{25} & H^{*'}_{26} & H^{*'}_{27} \\ H^{*'}_{31} & H^{*'}_{32} & H^{*'}_{33} & H^{*'}_{34} & H^{*'}_{35} & H^{*'}_{36} & H^{*'}_{37} \\ H^{*}_{41} & H^{*}_{42} & H^{*}_{43} & H^{*}_{44} & H^{*}_{45} & H^{*}_{46} & H^{*}_{47} \\ H^{*}_{51} & H^{*}_{52} & H^{*}_{53} & H^{*}_{54} & H^{*}_{55} & H^{*}_{56} & H^{*}_{57} \\ H^{*}_{61} & H^{*}_{62} & H^{*}_{63} & H^{*}_{64} & H^{*}_{65} & H^{*}_{66} & H^{*}_{67} \\ H^{*}_{71} & H^{*}_{72} & H^{*}_{73} & H^{*}_{74} & H^{*}_{75} & H^{*}_{76} & H^{*}_{77} \end{bmatrix} . \tag{31}$$

Using the compliance matrix, the displacement at each position of the mount coordinates can be derived using Eq. (32).

$$q' = \mathrm{H}^{*'} W + \mathrm{H}^{*'} F . \tag{32}$$

Based on Eq. (32), the response can be expressed in terms of the compliance matrix, excitation force, and control force, which implies that the motion of each position can be expressed in terms of the amplitude of the excitation force, the amplitude of the control force, and the phase. The displacement of each position is expressed as shown in Eq. (33).

$$\xi_j^*(t)=\left(\Xi_{mj}^{z*}e^{i\beta_{mj}}+\Xi_{mj.ac1}^{z*}e^{i\left(\phi_{ac1}+\beta_{mj.ac1}\right)}+\Xi_{mj.ac2}^{z*}e^{i\left(\phi_{ac2}+\beta_{mj.ac2}\right)}\right)e^{i\omega t}. \quad (33)$$

Here, Ξ_{mj}^{z*} is the amplitude arising from the excitation force among the displacement responses at position j (index number, 1 or 2), β_{mj} the phase caused by the excitation force, $\Xi_{mj.ac1}^{z*}$ the amplitude arising from the vertical mount control force, $\beta_{mj.ac1}$ the phase caused by the vertical mount control force, $\Xi_{mj.ac2}^{z*}$ the amplitude of the horizontal mount control force, and $\beta_{mj.ac2}$ the phase arising from the horizontal mount control force. These amplitudes and phases can be calculated using the compliance matrix, as expressed in Eqs. (34)-(37).

$$\Xi_{mj}^{z*}=\left(H_{j1}^{*'}+H_{j6}^{*'}d\right)W^z \quad (34)$$

$$\Xi_{mj.ac1}^{z*}=H_{j3}^{*'}f_{ac1}^z,\ \Xi_{mj.ac2}^{z*}=H_{j5}^{*'}f_{ac2}^x \quad (35)$$

$$\beta_{mj}=\angle\left(H_{j1}^{*'}+H_{j6}^{*'}d\right) \quad (36)$$

$$\beta_{mj.ac1}=\angle H_{j3}^{*'},\ \beta_{mj.ac2}=\angle H_{j5}^{*'}. \quad (37)$$

Based on Eq. (32), which represents the displacement, all the variables are known, except for the amplitude and phase of the vertical and horizontal mount control forces. To obtain a zero displacement, the phases of the control forces are assumed to be equal, as shown in Eq. (38).

$$\beta_{mj}=\beta_{mj.ac1}+\varnothing_{ac1},\ \beta_{mj}=\beta_{mj.ac2}+\varnothing_{ac2}. \quad (38)$$

Using Eq. (38), the phases in which the vertical and horizontal mounts should have appeared are expressed as shown in Eq. (39).

$$\varnothing_{ac1}=\beta_{mj}-\beta_{mj.ac1},\ \varnothing_{ac2}=\beta_{mj}-\beta_{mj.ac2}. \quad (39)$$

Substituting Eq. (39) into Eq. (32) yields Eq. (40).

$$\xi_j^*(t)=\left(\Xi_{mj}^{z*}+\Xi_{mj.ac1}^{z*}+\Xi_{mj.ac2}^{z*}\right)e^{i(\omega t+\beta_{mj})}. \quad (40)$$

Because the two unknowns cannot be obtained using only Eq. (40), the amplitudes of the vertical and horizontal mounts are calculated by adding an equation that yields a zero displacement at position k. The secondary path input is expressed as shown in Eqs. (41) and (42).

$$\varnothing_{ac1}=\beta_{mk}-\beta_{mk.ac1},\ \varnothing_{ac2}=\beta_{mk}-\beta_{mk.ac2} \quad (41)$$

$$\xi_k^*(t)=\left(\Xi_{mk}^{z*}+\Xi_{mk.ac1}^{z*}+\Xi_{mk.ac2}^{z*}\right)e^{i(\omega t+\beta_{mk})}. \quad (42)$$

The equations are arranged to calculate the amplitudes of the vertical and horizontal mounts that render the amplitudes of Eqs. (40) and (42) zero, as shown in Eq. (43).

$$\Xi_{mj}^{z*}+\Xi_{mj.ac1}^{z*}+\Xi_{mj.ac2}^{z*}=0,\ \Xi_{mk}^{z*}+\Xi_{mk.ac1}^{z*}+\Xi_{mk.ac2}^{z*}=0. \quad (43)$$

In Eq. (43), the element due to the exciting force is transposed to the right side, and by substituting Eqs. (34) and (35) and converting to the matrix form, Eq. (44) is derived.

$$\begin{bmatrix}H_{j3}^{*'} & H_{j5}^{*'}\\ H_{k3}^{*'} & H_{k5}^{*'}\end{bmatrix}\begin{Bmatrix}f_{ac1}^z\\ f_{ac2}^x\end{Bmatrix}=-W^z\begin{Bmatrix}H_{j1}^{*'}+H_{j6}^{*'}d\\ H_{k1}^{*'}+H_{k6}^{*'}d\end{Bmatrix}. \quad (44)$$

If the inverse matrix of the matrix comprising only the compliance elements on the left side of Eq. (44) is multiplied by the left- and right-hand sides, then the amplitudes required for the vertical and horizontal mounts can be derived using Eqs. (45) and (46).

$$f_{ac1}^z=W^z\left(\frac{\left|H_{j5}^{*'}\right|\left|H_{k1}^{*'}+H_{k6}^{*'}d\right|-\left|H_{k5}^{*'}\right|\left|H_{j1}^{*'}+H_{j6}^{*'}d\right|}{\left|H_{j3}^{*'}\right|\left|H_{k5}^{*'}\right|-\left|H_{j5}^{*'}\right|\left|H_{k3}^{*'}\right|}\right) \quad (45)$$

$$f_{ac2}^x=W^z\left(\frac{\left|H_{k5}^{*'}\right|\left|H_{j1}^{*'}+H_{j6}^{*'}d\right|-\left|H_{j5}^{*'}\right|\left|H_{k1}^{*'}+H_{k6}^{*'}d\right|}{\left|H_{j3}^{*'}\right|\left|H_{k5}^{*'}\right|-\left|H_{j5}^{*'}\right|\left|H_{k3}^{*'}\right|}\right). \quad (46)$$

Therefore, to control the displacement of position j to zero, the control force with the phase value derived from Eq. (39) and the amplitude values derived from Eqs. (45) and (46) is input to the secondary path. To control the displacement of position k to zero, the control force with the phase value derived from Eq. (41) and the amplitude values derived from Eqs. (45) and (46) must be input to the secondary path. To calculate the secondary path input value, two positions among the four vertical displacements must be combined. Thus, six methods are applied: (1) targeting two displacements of the source, (2) targeting two displacements of the receiver, (3) targeting the receiver displacement adjacent to the vertical mount and the displacement of the source adjacent to the horizontal mount, (4) targeting the source displacement adjacent to the vertical mount and the receiver displacement adjacent to the horizontal mount, (5) targeting the displacement to the left of the source and receiver, and (6) targeting the displacement to the right of the source and receiver.

4. Numerical validation

4.1 Conditions for simulation

Before conducting an experiment to demonstrate the model and validate the formulas derived above, a simulation was conducted to validate the performance of the model. The parameters used in the simulation are listed in Table 1. These values are based on the following experimental setup, which will be utilized for the experimental validation of the simulation results as a future work. Masses and inertias are measured and calculated. Stiffness and damping values are estimated by a series of experiment: a chirp voltage signal excites the stack mass, and an accelerometer measures the response. This results in a single resonance peak and based on this, the stiffness value is estimated with the natural frequency formulation and half power method.

Table 1. Parameters used in validation.

Variable	Value	Unit
m_1	1.721	kg
m_2	1.350	kg
m_{ac1}	0.075	kg
m_{ac2}	0.067	kg
I_1^y	33.402	gm^2
I_2^y	18.070	gm^2
k_{m1}^z	5.46	kN/mm
$k_{m2}^z = k_{m2}^x = k_{m2}^{zx}$	2.48	kN/mm
k_{m3}^z	0.61	kN/mm
$k_{m4}^z = k_{m4}^x = k_{m4}^{zx}$	0.53	kN/mm
$k_{b1}^z = k_{b2}^z$	0.42	kN/mm
c_{m1}^z	22	Ns/m
$c_{m2}^z = c_{m2}^x = c_{m2}^{zx}$	14	Ns/m
c_{m3}^z	64	Ns/m
$c_{m4}^z = c_{m4}^x = c_{m4}^{zx}$	48	Ns/m
$c_{b1}^z = c_{b2}^z$	200	Ns/m
$l_{s1} = l_{s3}$	50.686	mm
l_{s2}	179.314	mm
$l_{r1} = l_{r2}$	136	mm
$l_{r3} = l_{r5}$	0	mm
l_{r4}	200	mm
d	50	mm

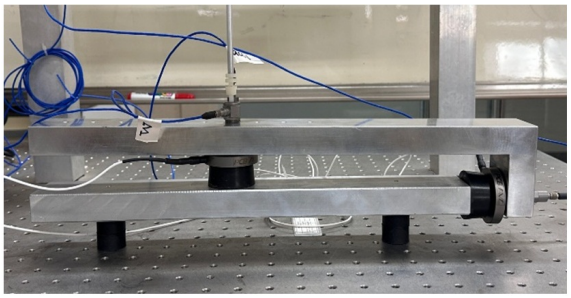

Fig. 8. Experimental setup used for parameter determination.

Vertical and horizontal mounts were placed at the CG of the source and receiver, respectively, and a simulation was performed by applying the calculated input value for the second path. The response was investigated using the linear time-invariant state–space method, and the vibration reduction performance was analyzed by comparing the response when only the excitation force was applied and when both the excitation force and the calculated control input were applied. The state-space equation is shown in Eqs. (47)-(49) using the mass–damping–spring motion equation converted to the mount coordinates shown in Eq. (19).

$$\dot{x}(t) = Ax(t) + Bu(t) \tag{47}$$

$$y(t) = Cx(t) + Du(t) \tag{48}$$

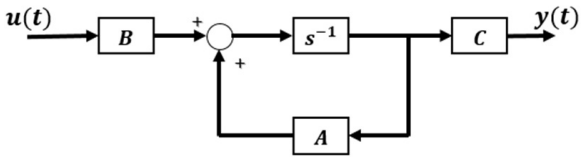

Fig. 9. Block diagram of state–space method.

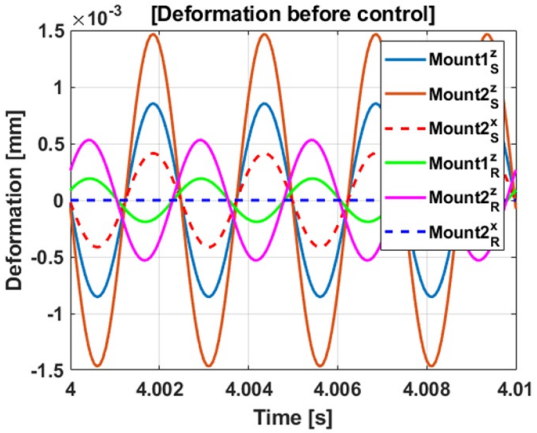

Fig. 10. Steady-state response graph for harmonic excitation force.

$$A = \begin{bmatrix} 0_{7\times7} & I_{7\times7} \\ -M'^{-1}K' & -M'^{-1}C' \end{bmatrix}, \quad B = \begin{bmatrix} 0_{7\times7} \\ -M'^{-1} \end{bmatrix}$$

$$C = \begin{bmatrix} I_{2\times2} & 0_{2\times3} & 0_{2\times2} & 0_{2\times7} \\ 0_{2\times2} & 0_{2\times3} & I_{2\times2} & 0_{2\times7} \end{bmatrix}, \quad D = 0\,. \tag{49}$$

In Eq. (49), matrix A represents the state of the system, matrix B the input, matrix C the output, and matrix D the direct transfer term. In this model, as no directly transferred elements are present, matrix D is represented as a zero matrix. The output of the simulation is expressed as the displacement of the position adjacent to the mount by appropriately adjusting the state variable, as expressed in Eq. (50).

$$y(t) = \left[\xi_{m1}^z(t) \quad \xi_{m2}^z(t) \quad \xi_{m3}^z(t) \quad \xi_{m4}^z(t)\right]^T. \tag{50}$$

To provide better understanding of the state–space method, a block diagram is shown in Fig. 9.

For the secondary path input simulation, the sampling frequency was set to 15000 Hz, the excitation frequency to 400 Hz, and the excitation amplitude to a sinusoidal signal with an amplitude of 10 N. A sinusoid, rather than more realistic signal created from automotive vehicles, is employed to see the feasibility and the characteristics of response from the created control input signal. Fig. 10 shows each displacement response when only the excitation force was input into the 7-DOF model before substituting the calculated secondary path input.

$Mount(i)_s^z$ is the vertical displacement of the i-th source position based on the left side of the mount coordinates,

Table 2. Case classification with respect to targets.

Case	#1	#2	#3	#4	#5	#6
Path 1	Position 1	Position 4	Position 4	Position 1	Position 1	Position 2
Path 2	Position 2	Position 5	Position 2	Position 5	Position 4	Position 5

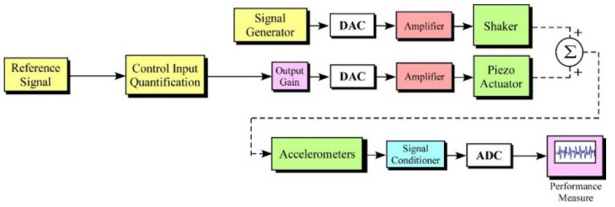

Fig. 11. Conceptual block diagram for the implementation of active vibration control.

$Mount2_s^x$ the horizontal displacement of the source adjacent to the horizontal mount, $Mount2_R^z$ the vertical displacement of the first receiver position, and $Mount2_R^x$ the horizontal displacement of the receiver adjacent to the horizontal mount. Fig. 10 shows that when the control force is not input through the secondary path, vibration is severe in the source directly affected by the excitation force; in particular, $Mount2_S^z$, which is distant from the CG, is susceptible to vibration. Hence, the vibration reduction performance was investigated by substituting the secondary-path input values calculated using the six methods described above.

The conceptual block diagram for active vibration control is shown in Fig. 11 for better understanding. The excitation force from the electrodynamic shaker is applied to the upper plate and transmitted to the lower plate through paths. An RCP system is used to make input signal to the shaker and the quantified signal to the piezoelectric actuators. Also, it works as a data acquisition system to gather acceleration signals of the structure.

4.2 Simulation results

For each method, the 7-DOF vibration reduction performance was compared based on a steady-state response plot and the root mean square of the steady-state response. The cases, classified into six categories, are summarized in Fig. 12 and Table 2.

The sensors used here are accelerometers. Since the control strategy proposed in this work is a feedforward control, all the sensors implemented are for performance measure with acceleration of each position. However, for this work, displacements for each position will be compared for evaluating vibration attenuation performance. In Fig. 12, position 1 is the response of $Mount1_S^z$, position 2 the response of $Mount2_S^z$, position 3 the response of $Mount2_S^x$, position 4 the response of $Mount1_R^z$, and position 5 the response of $Mount2_R^z$ and $Mount2_R^x$ in the steady-state response graph. Path i in Table 2 is the position where the vertical displacement is targeted to be zero in each case, and 12 types of simulations were conducted

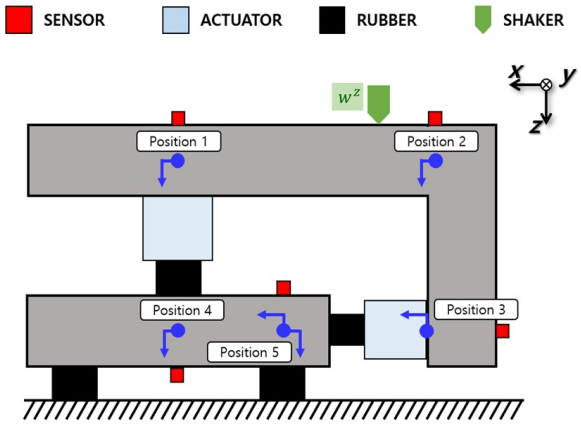

Fig. 12. Position definition for vibration measurement.

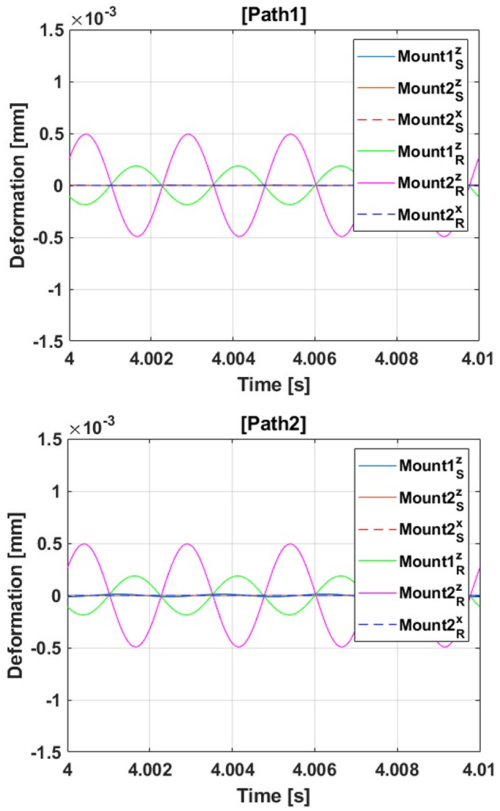

Fig. 13. Controlled steady-state response in case 1.

using two detailed methods in one case.

First, the control results of case 1 (targeting two displacements of the source as “0”) are shown in the steady-state response graph in Fig. 13 and Table 3, and the RMS values before and after control were compared.

In case 1, both displacements of the targeted source were effectively controlled; however, the vibration of the receiver worsened. Meanwhile, the vibration of the vehicle engine was controlled; however, the vibration of the subframe, which directly affects the occupants, was not controlled. Fig. 14 and Table 4 show the control results of case 2 (targeting two dis-

Table 3. Comparison of RMS values in case 1.

[Unit: μm]	Source		
	$Mount1_S^z$	$Mount2_S^z$	$Mount2_S^x$
Before control	0.6038	1.0373	0.2932
Path 1	0 100 % ↓	0.0021 99.8 % ↓	0.0005 99.8 % ↓
Path 2	0.0099 98.4 % ↓	0 100 % ↓	0 100 % ↓
[Unit: μm]	Receiver		
	$Mount1_R^z$	$Mount2_R^z$	$Mount2_R^x$
Before control	0.0534	0.188	1.39×10^{-7}
Path 1	0.1318 146.9 % ↑	0.349 85.64 % ↑	5.14×10^{-7} 269.9 % ↑
Path 2	0.132 147.2 % ↑	0.349 85.64 % ↑	5.14×10^{-7} 270 % ↑

Table 4. Comparison of RMS values in case 2.

[Unit: μm]	Source		
	$Mount1_S^z$	$Mount2_S^z$	$Mount2_S^x$
Before control	0.6038	1.0373	0.2932
Path 1	2.2848 278.4 % ↑	2.9591 185.3 % ↑	0.8364 185.3 % ↑
Path 2	2.2885 279 % ↑	2.9634 185.7 % ↑	0.8376 185.7 % ↑
[Unit: μm]	Receiver		
	$Mount1_R^z$	$Mount2_R^z$	$Mount2_R^x$
Before control	0.0534	0.188	1.39×10^{-7}
Path 1	0 100 % ↓	0.014 92.52 % ↓	6.05×10^{-10} 99.56 % ↓
Path 2	0.0005 98.96 % ↓	0 100 % ↓	0 100 % ↓

placements of the receiver as “0”).

In case 2, the two displacements of the target receiver were effectively controlled; however, the vibration of the source worsened. This is the opposite of the result of case 1 but the vibration of the subframe that directly affects the occupant was controlled; however, the vibration of the engine worsened.

Fig. 15 and Table 5 show the control results of case 3 (where the receiver displacement adjacent to the vertical mount and the source displacement adjacent to the horizontal mount are “0”).

For case 3, path 1 controlled only the displacement of the receiver adjacent to the target vertical mount, thereby increasing the displacements at other points. Similarly, in path 2, only the source adjacent to the target horizontal mount was mitigated, whereas the vibration at the other points was aggravated. This occurred because the amplitude of the control force was larger than that of the excitation force entering the secondary path input. This method aggravates the vibrations of the engine and subframe of the vehicle.

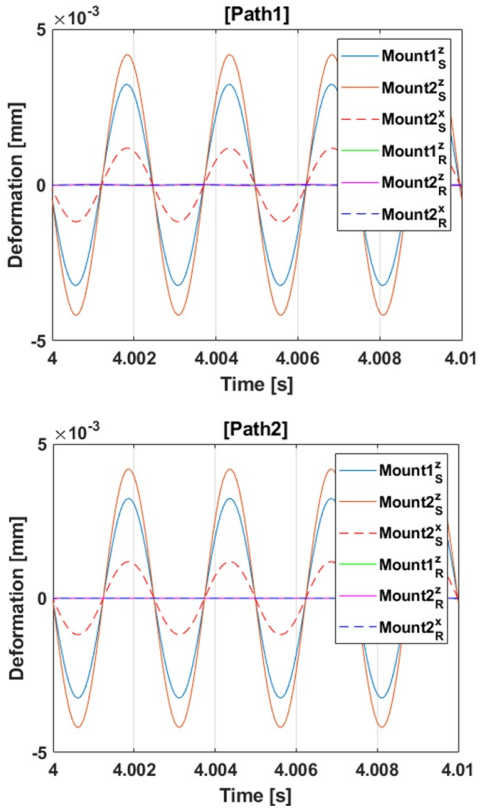

Fig. 14. Controlled steady-state response in case 2.

Fig. 16 and Table 6 show the control results of case 4 (where the source displacement adjacent to vertical mount and the receiver displacement adjacent to the horizontal mount are “0”).

In path 1 of case 4, the vibration of the source reduced, whereas that of the receiver exacerbated. In path 2, the displacement of the receiver adjacent to the target horizontal mount and the vibration at the left of the source reduced; however, the vibration t other points deteriorated.

Fig. 17 and Table 7 show the control results of case 5 (where the target left displacement of the source and receiver is “0”).

In case 5, the vibration at the target point, as well as at other points, was alleviated. This can improve the NVH performance of the vehicle and the stability of the engine by reducing the vibration of the engine and subframe.

Finally, Fig. 18 and Table 8 show the control results of case 6 (where the right displacement of the source and receiver is set to “0”).

For case 6, the result shows the same tendency as case 4, i.e., in path 1, the vibration of the source reduced, and the vibration of the receiver deteriorated. In path 2, the displacement of the receiver adjacent to the target horizontal mount and the vibration at the left of the source reduced; however, the vibration at other points deteriorated. When the displacement of the horizontal active mount and the adjacent position were con-

Table 5. Comparison of RMS values in case 3.

[Unit: μm]	Source		
	$Mount1_S^z$	$Mount2_S^z$	$Mount2_S^x$
Before control	0.6038	1.0373	0.2932
Path 1	6.3047 944 % ↑	6.8058 556 % ↑	1.9237 556 % ↑
Path 2	4.241 602 % ↑	0 100 % ↓	0 100 % ↓
[Unit: μm]	Receiver		
	$Mount1_R^z$	$Mount2_R^z$	$Mount2_R^x$
Before control	0.0534	0.188	1.39×10^{-7}
Path 1	0 100 % ↓	0.2483 32 % ↑	1.89×10^{-7} 35.9 % ↑
Path 2	0.8241 1443 % ↑	1.1883 532 % ↑	7.32×10^{-6} 5173 % ↑

Table 6. Comparison of RMS values in case 4.

[Unit: μm]	Source		
	$Mount1_S^z$	$Mount2_S^z$	$Mount2_S^x$
Before control	0.6038	1.0373	0.2932
Path 1	0 100 % ↓	0.064 93.83 % ↓	0.0181 93.83 % ↓
Path 2	0.4784 20.76 % ↓	1.6398 58.09 % ↑	0.4635 58.09 % ↑
[Unit: μm]	Receiver		
	$Mount1_R^z$	$Mount2_R^z$	$Mount2_R^x$
Before control	0.0534	0.188	1.39×10^{-7}
Path 1	0.1209 126.6 % ↑	0.3317 76.45 % ↑	4.60×10^{-7} 231 % ↑
Path 2	0.0706 32.32 % ↑	0 100 % ↓	0 100 % ↓

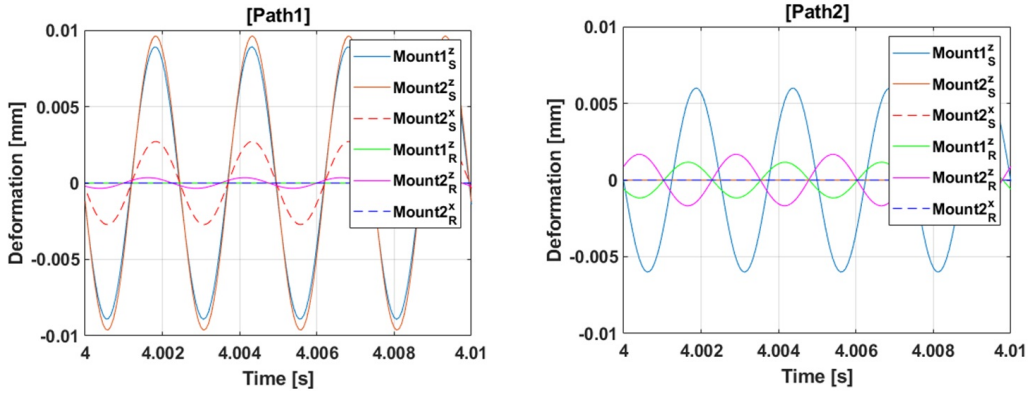

Fig. 15. Controlled steady-state response in case 3.

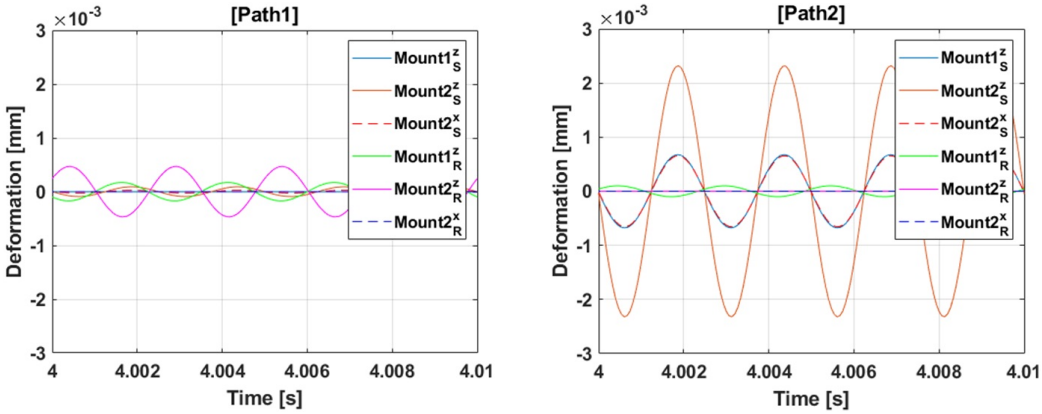

Fig. 16. Controlled steady-state response in case 4.

trolled to zero in each case, a relatively large control force was required, which deteriorated the vibration reduction performance.

When controlling for case 5, the overall vibration reduced. In cases 1, 3, and 6, when one structure was controlled, the other deteriorated. When controlling for cases 2 and 4, a control force exceeding the external force was necessary, and vibration occurred at locations other than the target, which implies worse performance. The simulation results presented above indicate that horizontally active mounts require more control

Table 7. Comparison of RMS values in case 5.

[Unit: μm]	Source		
	$Mount1_S^z$	$Mount2_S^z$	$Mount2_S^x$
Before control	0.6038	1.0373	0.2932
Path 1	0 100 % ↓	0.6709 35.32 % ↓	0.1896 35.32 % ↓
Path 2	0.0912 84.89 % ↓	0.8177 21.17 % ↓	0.2311 21.17 % ↓
[Unit: μm]	Receiver		
	$Mount1_R^z$	$Mount2_R^z$	$Mount2_R^x$
Before control	0.0534	0.188	1.39×10^{-7}
Path 1	0.0184 65.45 % ↓	0.1676 10.84 % ↓	9.48×10^{-8} 31.74 % ↓
Path 2	0 100 % ↓	0.1385 26.34 % ↓	5.87×10^{-8} 57.7 % ↓

Table 8. Comparison of RMS values in case 6.

[Unit: μm]	Source		
	$Mount1_S^z$	$Mount2_S^z$	$Mount2_S^x$
Before control	0.6038	1.0373	0.2932
Path 1	0.2651 56 % ↓	0 100 % ↓	0 100 % ↓
Path 2	0.1631 72.99 % ↓	1.4092 35.86 % ↑	0.3983 35.86 % ↑
[Unit: μm]	Receiver		
	$Mount1_R^z$	$Mount2_R^z$	$Mount2_R^x$
Before control	0.0534	0.188	1.39×10^{-7}
Path 1	0.0891 66.98 % ↑	0.2966 57.78 % ↑	3.50×10^{-7} 151.98 % ↑
Path 2	0.0828 32.32 % ↑	0 100 % ↓	0 100 % ↓

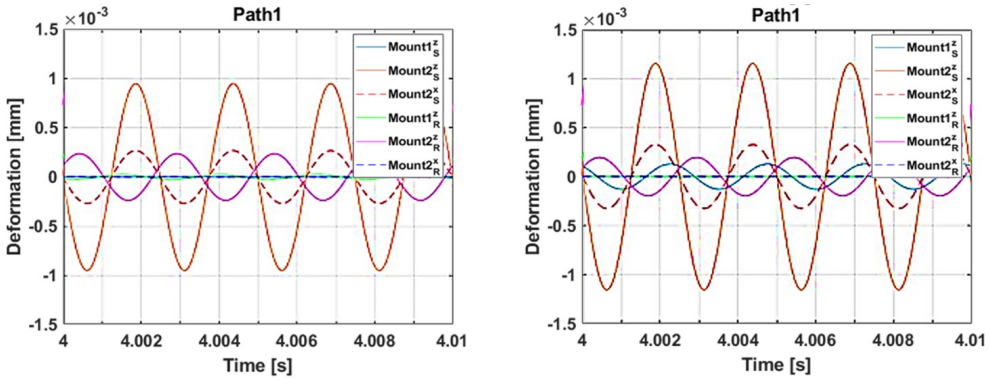

Fig. 17. Controlled steady-state response in case 5.

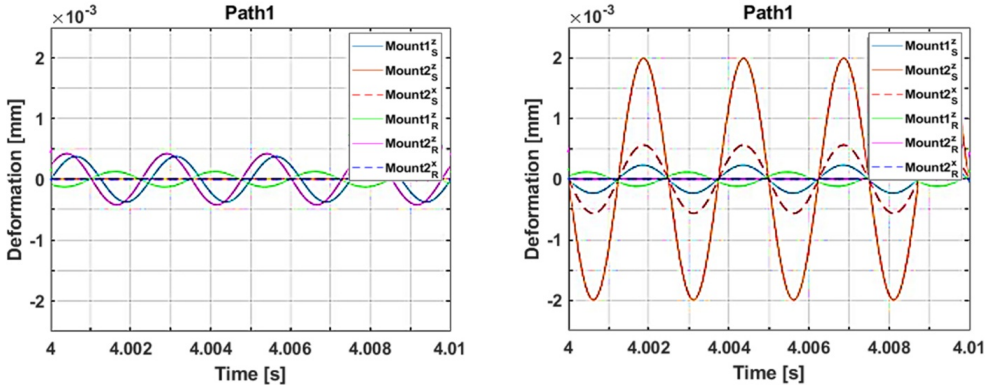

Fig. 18. Controlled steady-state response in case 6.

than vertical mounts.

5. Conclusions

In this study, an engine mount between an engine and a vehicle subframe was designed by combining a piezo actuator and an elastomer. Subsequently, the vibration reduction performance was analyzed with orienting the mount positions in the similar direction of realistic automotive mounting system. By setting the vehicle engine as the source, the active mount as the path, and the subframe as the receiver, the entire structure was designed and simulated as a source–path–receiver system. For a sinusoidal signal, the vibration reduction effect was validated by calculating the amplitude and phase required

for each active mount.

The vibration reduction effect of the structure was investigated using a 7-DOF model with both vertical and horizontal active mounts. Regarding the response in the horizontal direction, the dynamic relational expression was used to identify a trend and a method to control it. The vibration reduction effect was summed for six input control forces when a sine wave was introduced, and the control force of each active mount was calculated. Vibration reduction in the entire structure was demonstrated in certain cases. The result confirmed that the vibration at a location near the source's CG and the vibration of the receiver reduced significantly, thereby enhancing the NVH performance.

The contributions of this research are as follows.

1) A general approach for examining the vibrational motion of mounting structure, which includes the lumped parameter modeling and the actuator input quantification, is suggested so that it can be applied and expanded to any type of mounting systems. It would be also useful to determine the optimized location of the mounts and the actuation strategy.

2) Both vertical and lateral vibration of automotive mount inspired structure are investigated and their interactions are observed, while prior studies primarily focused on the actuation method and the vibration attenuation in one direction only.

3) According to targeted positions for the quantification of actuator input, vibration attenuation performance is compared and discussed. This would be also helpful to make the actuation strategy.

As future works, the results of this work should be validated throughout experiments with various control strategies including skyhook damping and with various disturbances including white noise. In addition, it is planned to demonstrate the effect of the coupling direction of the engine mount on the source and receiver for facilitating more efficient control. Finally, the constitutive relationship o the piezoelectric actuator and the nonlinearities of passive mounts (rubbers) should be considered in the future to express the motional behavior of the active mounting system more accurate so that the vibration control performance could be much more enhanced.

Acknowledgments

This work was supported by Basic Science Research Program through the National Research Foundation of Korea (NRF) funded by the Ministry of Education (NRF-2022R1 F1A1076089) and also supported by the 2022 Yeungnam University Research Grant (222A380002).

Nomenclature

m : Mass
I : Inertia
l : Distance
k : Stiffness
ε : Displacement
ξ : Displacement at each actuator part
θ : Rotational displacement
w : Shaker force
f : Actuator force
μ : Step size (mu)
a : Output signal at each actuator path
M : Mass matrix
C : Damping matrix
K : Stiffness matrix
W : Shaker force vector
F : Actuator force vector
q : Displacement vector
c : Damping coefficient
φ : Phase
ω : Frequency
k : Dynamic stiffness matrix
H : Compliance matrix
θ : Amplitude
β : Phase

Superscripts, subscripts

1 : Upper structure (source)
2 : Lower structure (receiver)
aci : Actuator
sti : Stack actuator
f : Flank
x : X-direction
y : Y-direction
z : Z-direction
gi : Actuator position
$*$: Complex number

References

[1] Y. Yu, N. G. Naganathan and R. B. Dukkipati, A literature review of automotive vehicle engine mounting systems, *Mechanism and Machine Theory*, 36 (1) (2001) 123-142.

[2] M. Hosseini, S. Arzanpour, F. Golnaraghi and A. M. Parameswaran, Solenoid actuator design and modeling with application in engine vibration isolators, *Journal of Vibration and Control*, 19 (7) (2012) 1015-1023.

[3] R. Kraus, S. Herold, J. Millitzer and T. Jungblut, Development of active engine mounts based on piezo actuators, *ATZ Peer Review*, 116 (2014) 50-55.

[4] H. D. Chae and S. B. Choi, A new vibration isolation bed stage with magnetorheological dampers for ambulance vehicles, *Smart Materials and Structures*, 24 (2015) 0964-1726.

[5] T. J. Yang, Z. J. Suai, Y. Sun, M. G. Zhu, Y. H. Xiao, X. G. Liu, J. T. Du, G. Y. Jin and Z. G. Liu, Active vibration isolation system for a diesel engine, *Noise Control Engr. J.*, 60 (3) (2012) 267-282.

[6] J. Jeon, Y. M. Han, D. Y. Lee and S. B. Choi, Vibration control of the engine body of a vehicle utilizing the magnetorheological roll mount and the piezostack right-hand mount, *Proc. Inst. of Mech. Eng. Part D: Journal of Automobile Engineering*, 227 (11) (2013) 1-16.

[7] J. Jiang, W. Gao, L. Wang, Z. Teng and Y. Liu, Active vibration control based on modal controller considering structure actuator interaction, *Journal of Mechanical Science and Technology*, 32 (8) (2018) 3515-3521.
[8] V. Fakhari, S. B. Choi and C. H. Cho, A new robust adaptive controller for vibration control of active engine mount subjected to large uncertainties, *Smart Materials and Structures*, 24 (4) (2015) 045044.
[9] M. Elahinia, C. Ciocanel, M. Nguten and S. Wang, MR and ER based semiactive engine mounts, *Smart Materials Research*, 21 (2013) 831017.
[10] W. Wu, X. Chen and Y. Shan, Analysis and experiment of a vibration isolator using a novel magnetic spring with negative stiffness, *Journal of Sound and Vibration*, 333 (2014) 2958-2970.
[11] T. Q. Truong and K. K. Ahn, A new type of semi-active hydraulic engine mount using controllable area of inertia track, *Journal of Sound and Vibration*, 329 (2010) 247-260.
[12] T. Kamada, T. Fujita, T. Hatayama, T. Arikabe, N. Murai, S. Aizawa and K. Tohyama, Active vibration control of frame structures with smart structures using piezoelectric actuators (vibration control by control of bending moments of columns, *Smart Materials and Structures*, 6 (1997) 448-456.
[13] T. Loukil, O. Bareille, M. N. Ichchou and M. Haddar, A low power consumption control scheme: application to a piezostack-based active mount, *Frontiers of Mechanical Engineering*, 8 (2013) 383-389.
[14] L. Sui and X. X. G. Shi, Piezoelectric actuator design and application on active vibration control, *Physics Procedia*, 25 (2012) 1388-1396.
[15] S. B. Choi and Y. T. Choi, Sliding mode control of a shear-mode type ER engine mount, *KSME International Journal*, 13 (1999) 26-33.
[16] C. Sarkar, H. Hirani and A. Sasane, Magnetorheological smart automotive engine mount, *International Journal of Current Engineering and Technology*, 5 (1) (2015) 419-428.
[17] Y. Chang, J. Zhou, K. Wang and D. Xu, A quasi-zero-stiffness dynamic vibration absorber, *Journal of Sound and Vibration*, 494 (2020) 115859.
[18] J. Liette, J. T. Dreyer and R. Singh, Interaction between two Paths for source mass motion control over mid-frequency range, *Journal of Sound and Vibration*, 333 (2014) 2369-2385.
[19] D. Hong and B. Kim, Modeling and analysis of active mounting system for a plate-type structure, *Korean Soc. Mech. Eng. A*, 41 (10) (2017) 915-921.
[20] D. Hong and B. Kim, Vibration reduction for modulated excitation using lumped parameter modeling and multi-channel NLMS algorithm for a structure with three active paths between plates, *Journal of Mechanical Science and Technology*, 33 (10) (2019) 4673-4680.
[21] D. Hong and B. Kim, Quantification of active structural path for vibration reduction control of plate structure under sinusoidal excitation, *Applied Sciences*, 9 (4) (2019) 711.
[22] Y. Qiu, D. Hong and B. Kim, Optimal placement criteria of hybrid mounting system for chassis in future mobility based on beam-type continuous smart structures, *Scientific Reports*, 13 (2023) 2317.
[23] F. Hausberg, C. Scheiblegger, P. Pfeffer, M. Plöchl, S. Hecker and M. Rupp, Experimental and analytical study of secondary path variations in active engine mounts, *Journal of Sound and Vibration*, 340 (2015) 22-38.
[24] R. Kraus, S. Herold, J. Millitzer and T. Jungblut, Development of active engine mounts based on piezo actuators, *ATZ Worldwide*, 116 (2014) 46-51.
[25] T. Bartel, S. Herold, D. Mayer and T. Melz, Development and testing of active vibration control systems with piezoelectric actuators, *6th ECCOMAS Conference on Smart Structures and Materials*, Torino, Italy (2013) 24-26.
[26] H. Li and R. M. Goodall, Linear and non-linear skyhook damping control laws for active railway suspensions, *Control Engineering Practice*, 7 (7) (1999) 843-850.
[27] K. Singal and R. Rajamani, Zero-energy active suspension system for automobiles with adaptive sky-hook damping, *J. Vib. Acoust.*, 135 (1) (2013) 011011.
[28] J. Emura, S. Kakizaki, F. Yamaoka and M. Nakamura, Development of the semi-active suspension system based on the sky-hook damper theory, *SAE Transactions: Journal of Passenger Cars*, 103 (6) (1994) 1110-1119.
[29] Y. Chai, F. Li, Z. Song and C. Zhang, Analysis and active control of nonlinear vibration of composite lattice sandwich plates, *Nonlinear Dynamics*, 102 (2020) 2179-2203.
[30] B. Kim, G. N. Washington and R. Singh, Control of incommensurate sinusoids using enhanced adaptive filtering algorithm based on sliding mode approach, *Journal of Vibration and Control*, 19 (8) (2013) 1265-1280.
[31] B. Kim, G. N. Washington and R. Singh, Control of modulated vibration using an enhanced adaptive filtering algorithm based on model-based approach, *Journal of Sound and Vibration*, 331 (18) (2012) 4101-4114.

Dongwoo Hong received his Ph.D. from the Department of Mechanical Engineering at the Yeungnam University, Republic of Korea. He is currently a Senior Researcher at the Daegu Mechatronics & Materials Institute. His research interests are smart structures, vibration control, and deep learning, especially in automotive NVH applications.

Hojoon Moon received his M.S. from the Department of Mechanical Engineering at the Yeungnam University, Republic of Korea. He is currently a full-time researcher at the Research Institute of Mechanical Technology at the Yeungnam University. His research interests are smart structures and vibration control for automotive mounting systems.

Byeongil Kim received his Ph.D. from the Department of Mechanical Engineering at the Ohio State University, USA. He is currently an Associate Professor at Yeungnam University, Republic of Korea. His research interests are active noise and vibration control, adaptive structures and NVH control based on deep learning in automotive, aerospace, and industrial applications.